Egyptian Journal of Aquatic Biology & Fisheries
Zoology Department, Faculty of Science,
Ain Shams University, Cairo, Egypt.
ISSN 1110 – 6131
Vol. 28(5): 2029 – 2049 (2024)
www.ejabf.journals.ekb.eg

Evaluation of Green-Synthesized Nanoparticles for their Activity against Marine Fouling Bacteria: A Promising Approach for Antimicrobial Coatings

Nayrah A. Shaltout*, Ehab A. Beltagy, Hassan Abdallah Ibrahim, Mohamed A. Aly-Eldeen
National Institute of Oceanography and Fisheries, NIOF, Egypt
***Corresponding author: nshaltout@gmail.com**

ARTICLE INFO

Article History:
Received: Sept. 18, 2024
Accepted: Oct. 3, 2024
Online: Oct. 30, 2024

Keywords:
Marine biofouling,
Nanoparticles,
Chitosan,
Algae,
Mangrove,
Antibacterial

ABSTRACT

The present study aimed to synthesize nanoparticles from several crude extracts of *Ulva fasciata* Delile, *Corallina mediterranea* Areschoug, *Jania rubens* (Linnaeus), *Pterocladiella capillacea* (S.G. Gmelin), and mangrove leaves of *Avicennia marina* (Forsk.), mixed with composites of chitosan and iron magnet. The efficiency of these synthesized nanoparticles was screened and evaluated against marine biofilm bacteria as a potential solution to combat biofouling in marine environments. The antimicrobial potential of these biosynthesized nanoparticles was assessed under optimal conditions of concentration and pH. Various techniques, including Fourier Transform Infrared Spectroscopy (FT-IR) analysis and Transmission Electron Microscopy (TEM), were used to characterize the chemical active groups and physical properties of the nanoparticles. The findings of this study revealed that the size of all the biosynthesized nanoparticles ranged between 2.16 and 18.50nm. They demonstrated high antibacterial activity against marine fouling bacteria, suggesting a promising eco-friendly alternative for biofouling control in marine environments. The data indicated that the nanocomposites of *J. rubens* and *C. mediterranea* with chitosan were the most effective in suppressing bacterial communities, while the composites with extracts from *A. marina* and *P. capillacea* exhibited very low efficiency. For metal-centered nanoparticles, the synthesized nanocomposite of iron with *J. rubens* and *U. fasciata* showed the highest antibacterial efficiency, followed by the composite with leaves of *A. marina* mangrove. Nanocomposites using magnet with all the crude extracts showed lower efficiency compared to those with iron. The study also revealed that increasing the concentration of crude extracts had no significant effect on the efficiency of the nanocomposites. Additionally, shifting the pH toward an alkaline medium (pH = 9) led to a decrease in the antibacterial efficiency of the biosynthesized nanoparticles. These findings clearly demonstrate that biosynthesized nanoparticles from algae extracts combined with iron or chitosan can be developed as highly efficient antibacterial agents against biofilm-forming bacteria.

INTRODUCTION

Marine fouling of submerged marine surfaces presents significant challenges for various marine activities, such as aquaculture and shipping. A crucial part of the fouling of marine surfaces is played by bacterial biofilms. These bacterial biofilms are complex microbial communities encased in a protective extracellular matrix. These biofilms,

frequently dominated by a large diversity of bacterial species, adhere tenaciously to substrates and create a challenging environment for traditional antifouling techniques **(Dobretsov & Thomason, 2011)**. The formation of bacterial biofilms on marine objects not only endangers a marine object's infrastructure and structural integrity but also raises maintenance expenses and fuel consumption. The need for sustainable alternatives is highlighted by the fact that conventional antifouling techniques frequently rely on biocides, which have negative environmental effects. It is becoming more and more necessary to create environmentally eco-friendly substitutes that effectively mitigate bacterial biofilm formation without causing harm to the aquatic ecosystem for the sick of a sustainable marine environment. This urges the development of environmentally friendly and effective antifouling strategies to mitigate the economic and ecological consequences associated with fouling. In this context, the utilization of green-synthesized nanoparticles derived from natural sources offers a promising avenue for sustainable antifouling solutions.

Marine plants such as macroalgae and mangrove are rich in bioactive compounds and have been recognized by different researchers **(Priyanka & Rajaram, 2023)** for their distinctive and diversified flora with unique properties. They are widely recognized for their high content of a wide spectrum of bioactive compounds such as polyunsaturated fatty acids, lipids, glycerols, peptides, flavonoids, terpenoids, alkaloids, quinones, sterols, polyketides and polysaccharides **(Abdelsalam *et al.*, 2022)**. These compounds were marked for their potent antimicrobial and consequently antifouling properties **(Zbakh *et al.*, 2012)**.

Nanoparticles have gained great scientific attention because of their exceptional physicochemical characteristics, which enable high efficiency and a broad range of chemical and biological applications. In green approaches, plant extracts containing natural polymers are used to synthesize these nanoparticles as an environmentally friendly substitute for conventional chemical treatments. Considering the nanoscale size of the nanomaterial, it has been shown that the high surface area-to-volume ratio provides significant interaction with microbes, consequently increasing their antimicrobial efficiency. This is the primary reason for the exceptionally high recorded activity. This explains why these nanomaterials are considered novel antimicrobial agents **(Rozman *et al.*, 2023)**.

Many researchers have used the aqueous extract of *Ulva* (formerly *Enteromorpha*) *compressa* to generate biocompatible silver nanoparticles. The aqueous extract acts as both a stabilizer and a reducing agent, preserving the nanosilver at the nanoscale and maintaining its bioactivity **(Wang *et al.*, 2014; Bensy *et al.*, 2022)**. Furthermore, it has been demonstrated that chitosan is non-toxic, biocompatible, and biodegradable, which is recognized for a very broad range of pharmaceutical and

environmental applications. Additionally, it is recorded as one of the most efficient antimicrobial substances against marine micro-organisms **(Confederat *et al*., 2021)**.

Nano mangrove particles, extracted and synthesized from mangrove plant materials, hold the promise of providing novel antifouling agents. Similarly, *Ulva* (*Enteromorpha*) *compressa*, a green macroalga abundant along coastal regions, is recognized for its bioactive chemical constituents, which have a high potential antifouling property **(Kumar *et al*., 2020; Confederat *et al*., 2021)**.

As a novel approach to combat marine bacterial biofilm formation on marine objects, this research aimed to systematically screen, compare, and optimize the synergistic antifouling efficacy of various iron nanoparticles derived from mangrove sources, along with four algal extracts (*Ulva fasciata*, *Corallina mediterranea*, *Jania rubens*, and *Pterocladiella capillacea*), and chitosan against fouling bacteria. This evaluation focuses on investigating the effectiveness of these nanoparticles in inhibiting the growth of fouling bacteria, which are the primary building blocks of adhesive biofilms. Additionally, we aimed to provide valuable insights into the development of sustainable and effective antifouling strategies.

MATERIALS AND METHODS

1. Collection of algal samples and mangrove plant

Fresh algal samples were collected at a longitude of 30° 07'E and a latitude of 31° 16'N, at a depth of 0.5 to 1 meter in Abu Qir Bay, located in the Alexandria Mediterranean Sea. The collection and preparation of the algae followed the protocol described by **Shaltout and Shams El-Dein (2015)**. The collected algae samples were first pre-washed *in situ* with seawater to eliminate any adhered sediments, epiphytes, and contaminants. The residual impurities were then rinsed with tap water. Clean algae was then stored at 4°C under refrigeration. Collected algae were subjected to microscopic identification according to **Aleem (1993)** using Herbarium sheets.

Four algal species were collected to represent two algal classes: the Rhodophyceae, which was represented by *Corallina mediterranea* (Areschoug), *Jania rubens* (Linnaeus), *Pterocladiella capillacea* (S.G.Gmelin), whereas the second class is the Chlorophyceae, which was represented by one species, *Ulva fasciata* (Delile). According to **Shaltout and Shams El-dein (2015)**, each species represented weighed a constant 250 grams after being air-dried at room temperature (25°C).

Regarding the fresh matured mangrove (*Avicennia marina* (Forssk.) Vierh) leaves were collected from Hurghada coastal area. The collected leaves were first washed with tap water, and then with distilled water to remove any attached salts or associated contaminants.

2. Biosynthesis of iron nanoparticles

Following the method described by **Abdelsalam *et al.* (2022)**, about 10g of finely cut mangrove leaves or the four algae species was placed and boiled in 100mL deionized water for one hour to extract the bioactive compounds. The resulting extract was then filtered with Whatman no.1 filter paper. Then a total of 10mL of collected filtrate was added to 90mL of iron chloride aqueous solution (0.001M $FeCl_3$) with continuous stirring for two hours. The resulted brownish solution is the indication of the synthesized nano-iron.

3. Biosynthesis of magnet nanoparticles

The magnet nanoparticles (MNPs) were prepared exactly following the previously mentioned protocol by **Predoi (2007)**. A solution of 0.3 M ferrous chloride (Fe^{2+}) and 0.15 M ferric chloride (Fe^{3+}) was prepared in deionized water to create a mixed iron solution. Approximately 200mL of 2.0 M NaOH was then added to the iron solution. This mixture caused a brown hue to change to black, indicating the formation of magnetite nanoparticles as a black precipitate. The precipitate was separated by decantation and washed multiple times. The resulting magnetite nanoparticles were mixed with 10mL of 0.2 M sodium ammonium. The suspension was centrifuged to collect the magnetic nanoparticle (MNP) powder, which was then dried at 50°C. For the biosynthesis of the magnetite nanoparticles, 10mL of either algae extract or mangrove extract was used instead of a chemical stabilizer. These extracts served a dual purpose: acting as a reductant and enhancing the biological activity of the magnetite nanoparticles.

4. Preparation of chitosan nanoparticles

Nanochitosan was prepared following the method adopted by **Tang *et al*. (2007)**, as chitosan is deacetylated at 85% NaCL of (98% purity) and tripolyphosphate (TPP) cations. About 40ml of 2.0% (v/v) acetic acid was used to dissolve 20mg of chitosan. After that, roughly 20 milliliters of sodium tripolyphosphate (0.75mg/ mL) was gradually added per drop while being constantly stirred. The formed suspension of chitosan nanoparticles was centrifuged for separation. The supernatant was discarded, and the collected nano-chitosan was air-dried for further use and analysis **(Abdelsalam *et al.*, 2022)**.

5. Characterization of biosynthesized nanoparticles

5.1. Fourier transform infrared spectroscopy (FT-IR) analysis

Initially, a UV-VIS spectrophotometer was applied to monitor 1mL of a nanoparticle solution that had been diluted with 1:20, v/v Milli Q water (between 300-700nm ranges with 10nm intervals). The solution was centrifuged at 10000g for 10min and the resulted pellets were re-dispersed in Milli Q water. To guarantee total separation of the generated nanoparticles, the centrifugation procedure and re-dispersion were carried out three times. FT-IR spectroscopy was used to characterize the dried purified

pellet in the diffuse reflectance mode at a resolution of $4cm^{-1}$ using KBr pellets. The generated nanoparticles were subjected to FT-IR analysis using a Thermo Nicolet AVATAR 300 FT-IR spectrometer and the KBr pellet method, covering the range of 4000 to $375cm^{-1}$.

5.2. Size and morphology of nanoparticles

The particle size and morphology of produced nanoparticles were analyzed by transmission electron microscope (Joel CX 100). A thin layer of the sample was applied to a copper grid coated in gold.

6. Antibacterial activity of crude extracts and biosynthesized nanoparticles

The antimicrobial efficiency of both green synthesized nano- particles under investigation were tested by applying well-cut diffusion technique according to **El-Sayed *et al*. (2014)**. According to **Abdelsalam *et al*. (2022)**, the efficiency of the synthesized nanoparticles was evaluated based on an analysis of how they can prevent the development of indicator marine bacteria. In plates containing fifty millimeters of nutrient agar medium, the indicator microorganisms were inoculated. Following solidification of the agar in the plate, the agar after wells were punched out using a 0:5cm cork borer. After being sterilized using an ultra-filtration technique with 0.22µl sterilized filters, approximately 100 microliters of the tested composite nanoparticles, nano iron, or crude extract were placed into each well. At the proper temperature, all plates were incubated for 48 hours. Following the 48-hour incubation period, the degree of bacterial growth inhibition was assessed by measuring the radius in millimeters of the clear zone surrounding each well (Y) and the control well (X) **(El-Sayed *et al*., 2014)**. The absolute unit for the clear zone (AU) was obtained according to the following equation **(Yang *et al*., 1992)**:

$$AU = Y^2\pi/X^2\pi$$

The suggested equation ($AU = Y^2\pi/X^2\pi$) by **(Yang *et al*., 1992)** was used to calculate the absolute unit for the clear zone.

RESULTS AND DISCUSSION

In addition to particle size, the stability and safety of chitosan nanoparticles (CNPs) influence their efficiency **(El-Naggar *et al*., 2022)**. For instance, the CNPs prepared were evaluated as promising versatile cationic polymeric nanoparticles. The chitosan nanoparticles were considered to be promising, adaptable cationic polymeric nanoparticles. Due to their non-toxicity, biodegradability, small size (30-40nm) and biocompatibility, the use of chitosan nanoparticles is recommended in a wide range of biological applications.

In addition, biosynthesized metal-based nanoparticles (NPs), such as iron and iron oxide nanoparticles (magnet nanoparticles), exhibited strong potential for antimicrobial activity. Research proved that the use of either iron nanoparticles or magnet nanoparticles is a promising solution to overcome antimicrobial resistance or biofilm formation as they can interact with multiple biological molecules and inhibit microbial growth **(Zúñiga-Miranda *et al.*, 2023)**. Recently, **Flieger *et al.* (2024)** indicated that iron oxide nanoparticles (IONPs) are being studied due to their strong potential for antimicrobial activity and low toxicity to humans, which suggests that they have potential applications in environmental protection. Indeed, the conditions and processes used during IONPs synthesis have an effect on the size, shape, and surface modification of the product, which in turn causes variations and uncertainties in its biological activity. However, in the current study, the four algal species and mangrove leaf extracts were used for CNP biosynthesis.

1. FTIR analysis

Characterization of chitosan nanoparticles

The FT-IR spectrum of Fig. (1) displays the FT-IR spectrum of chitosan nanoparticles. The spectrum revealed the usual characteristic absorption bands in the range reported previously to chitosan **(Venkatesan *et al.*, 2011)**, which are the rock's C-H stretching at 1411cm^{-1} and the carbonyl group (C=O) at 1740cm^{-1}. The stretching vibrations of N, H, and OH are responsible for the peaks observed at 3190cm^{-1} in chitosan nanoparticles. The N-H bending vibration of amide II is associated with a peak at 1533cm^{-1}, while the peak at 1379cm^{-1} is attributed to the –CH_3 symmetrical deformation mode (scissoring) in the amide group.

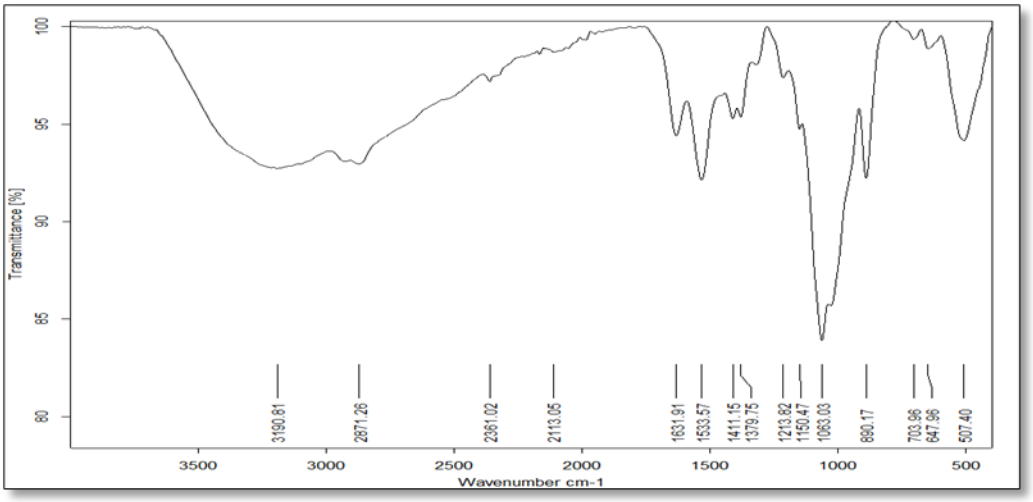

Fig. 1. FT-IR analysis for chitosan nanoparticles

The antisymmetric stretching of the C-O-C bridge is represented by the band at 1150, 1063, and 1150cm^{-1}, which is assigned to the stretching vibrations of the C-O-C

linkages in the polysaccharide structure. The peak at 2871.26cm^{-1} corresponds to the methyl group (CH_3), while that at 2361.02cm^{-1} is for the alkane group (CH). On the other hand, the alkene (C=C) is represented by the two peaks (1631.91 and 647.69cm^{-1}), and ether groups (C-O-C) are represented by the peak at 1031.73cm^{-1}. The identified peaks are the major functional groups in the following biologically active chemical compounds such as polyphenols, flavonoids, and terpenoids. These identified functional groups and the corresponding chemical classes were known by their very high chemical activity as a reducing agent. The high antimicrobial activity of terpenoids was attributed to their high ability to oxidize the aldehyde groups to carboxylic acids. Furthermore, polyphenols are also proven to have a potential reducing effect in the synthesis of silver nanoparticles **(Qi *et al.*, 2004)**.

FT-IR of biosynthesized iron nanoparticles using mangrove leaves

To determine the potential biomolecules and functional groups in charge of the Fe^{3+} ion reduction and bio-reduced FeNP capping processes, FT-IR measurements were performed.

Peaks in the FT-IR spectrum can be seen at 1220.36, 1023.87, 1536.02, 1373.90, 1628.10, and 775.90cm^{-1}. Upon analyzing the mangrove leaves bud extract's IR curve (Fig. 2), several broad peaks were observed at 2359.57cm^{-1}, which indicates the N-H stretching of any ammonium ions; a medium band at 1628.10cm^{-1} indicates the stretching of C = N; and a band at 1536cm^{-1} indicates the N-O stretching of nitro compounds.

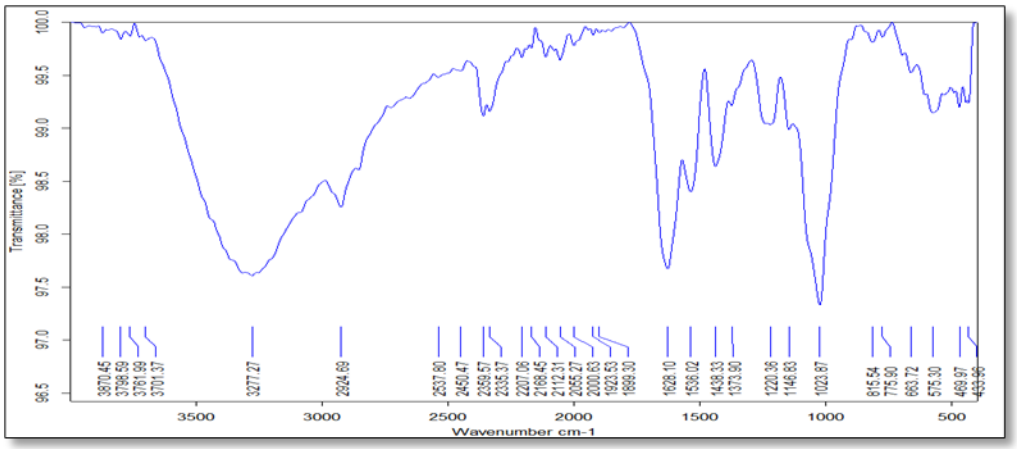

Fig. 2. FT-IR analysis for biosynthesized iron nanoparticles using *Avicennia marina* leaves extract

The N-O stretching of amide is also represented by the weaker band at 1373.90cm^{-1}; the C-X stretching of fluoroalkanes is represented by the broadband at 1023.87cm^{-1}; and the C-H stretching of aromatic benzene is represented by the strong band at 775.90cm^{-1}. Furthermore, a broad band at 3277cm^{-1} on the FeNPs curve, indicated the O-H stretching of high alcohol or phenol concentrations. The band located

at 2924.69cm^{-1} is ascribed to carboxylic acids' O-H stretching. The C-C stretching of aromatic C=C is represented by the weak to strong band at 1438.33cm^{-1} **(Abdelsalam *et al.*, 2022)**.

Additionally, the medium band at 1220.36cm^{-1} represents any carboxylic acid's C-O stretching. Alcohols, carboxylic acids, esters, and ethers were among the functional groups that effectively bound to the metal to form iron nanoparticles, according to the results of the FT-IR analysis. These groups have previously demonstrated that they possess certain reducing agents with the main chemical classes [flavonoids, triterpenoids, and polyphenols] in the synthesis of iron nanoparticles. It is worth noting that the C-N stretching and over-lapping of aliphatic amines and the N-H stretching vibration of primary amines have a stronger ability to bind metal. As a result, it is possible that the secondary metabolites from mangrove leaves will form a coat over the metal nanoparticles, preventing the particles from agglomerating and stabilizing in the medium. This evidence explains and agree with the findings of the antimicrobial efficiency obtained in this study, as the biological molecules perform for the reducing, capping and stabilizing of the metal colloids in an aqueous medium, hence achieve the highest biological activity.

Significantly, **Vaish and Pathak (2023)** recognized that mangrove plants hold great potential for the synthesis of bio-nanomaterials through the use of bioactive compounds. These plants can also be highly effective and beneficial for environmental applications. Biomolecules obtained from mangroves are used as precursors for the synthesis of nanoparticles in the production of bio-nanomaterials. The biocompatibility, low toxicity, and large surface area of these bio-nanomaterials make them advantageous for the sustainable use of mangroves.

Biosynthesized iron nanoparticles using Ulva fasciata

The FT-IR spectrum FeNPs molecule synthesized by *U. fasciata* extract showed that the functional group of the active ingredients was revealed by the *fasciata* extract. The functional groups of alkyl halides are represented by the peaks at 615.99 and 843.95cm^{-1} in the FT-IR analysis results (Fig. 3), while the peak at 928.98cm^{-1} is corresponding to the functional group of carboxylic acids. In addition, amides are represented by the recorded peak at 1631.71cm^{-1}, aromatics by the peak at 1442.14cm^{-1}, and aliphatic amines by the peaks at 1030.58cm^{-1}.

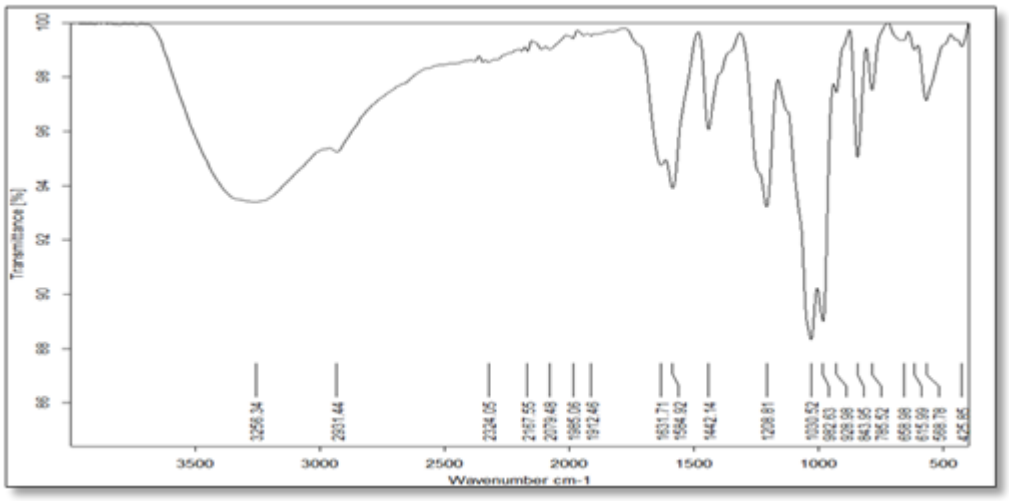

Fig. 3. FT-IR analysis for biosynthesized iron nanoparticles using *Ulva fasciata* extract

The primary and secondary amines' stretching vibrations were validated by these strong peaks that were recorded. Furthermore, the nitrile functional group is confirmed by the peak at 2324.05cm^{-1}, whereas the alcohol and phenol functional groups are represented by the peak at 425.85. It is clear from the spectrum that peaks corresponding to the hydroxyl, amino, and C-H groups were found close to the monomeric hydrogen bond's 3600–3000cm^{-1} O–H group, along with corresponding phenol rings. At 2079.48cm^{-1}, the C=C ring stretching was noticed. Gallic acid, alginic acid, flavonoids, tannins, and other phenols are identified by these IR spectra **(Abdelsalam *et al*., 2022)**. The solution's high biological antibacterial activity can be explained by the possibility that these soluble components served as stabilizing and reduction agents, preventing the aggregation of nanoparticles. **Bensy *et al*. (2022)** have also synthesized iron nanoparticles using *Ulva lactuca* water extract that was collected from the coast of Tamilnadu in India. The properties of their nanoparticles have been thoroughly studied.

Biosynthesized iron nanoparticles using Pterocladiella capillacea

FT-IR analysis was performed to determine the potential biomolecules accountable for the stabilization and reduction of Fe ions, as well as the capping of bio-reduced iron nanoparticles synthesized from *P. capillacea* extract (Fig. 4). The significant shift of the broad band at 3424cm^{-1} from *P. capillacea* extracts, as reported in **El-Rafie *et al*.(2013)**, to 3276.32 cm^{-1}, indicates the presence of polysaccharides, specifically the OH group of algal polysaccharides, and proteins, represented by the N-H groups of amide A and stretching of carboxylic acids. Additionally, the band at 2921.90cm^{-1} can be attributed to either secondary amine or alkane C-H bond stretching, while the bands at 1439.58cm^{-1} are assigned to carboxyl COO^{-} groups. Moreover, the absorption bands at 1631.12cm^{-1} can be accountable to either amide groups in proteins or carbonyl stretching in polysaccharides as previously recorded by **El-Rafie *et al*. (2013)**.

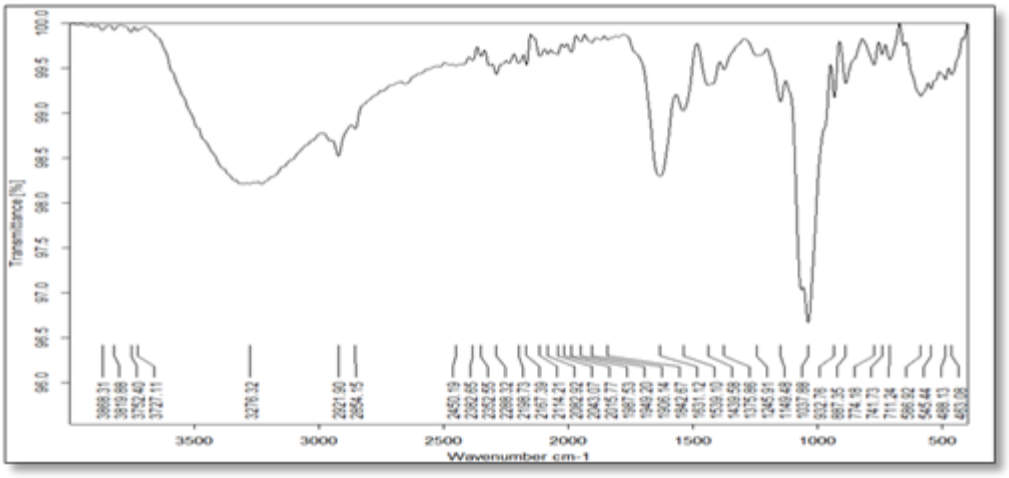

Fig. 4. FT-IR analysis for biosynthesized iron nanoparticles using *Pterocladiella capillacea* extract

The band at 1037cm^{-1} in *P. capillacea* extracts indicate the stretching of S=O of sulfated polysaccharides. It could be also representing the C-N bond stretch of aromatic amine groups. The peak at approximately 2300cm^{-1} could be due to the stretching of P-H bond in phospholipids or combination C-H stretching, C-N stretching, or the stretching vibration of -NH_2^+ and -NH_3^+. The peak at 1631.12cm^{-1} corresponds to the protein amide I band, primarily due to C=O stretching, while 1375.86cm^{-1} was attributed to protein (CH_2) and (CH_3) stretching of methyl carboxylic acid versus the (C-O) of COO^- groups those bonded to methyl $N(CH_3)_3$ in carboxylic lipids.

Previous research has indicated that proteins and amino acids have a higher capacity to bind metal due to their carbonyl groups. These results suggest that proteins may coat the metal nanoparticles to prevent agglomeration, stabilize the medium, and maintain the efficiency of the nanoparticles as the nano-size will not change **(Kanchana *et al*., 2011; El-Rafie *et al*., 2013)**. Additionally, the extracted polysaccharides include reducing sugars that can reduce silver and synthesize the nanoparticles via biogenic pathways **(El-Rafie *et al*., 2013)**.

Biosynthesized iron nanoparticles using Jania Rubens

The FT-IR spectroscopy for the bio-reduced synthesized nanoparticle prepared from *J. rubens* extract (Fig. 5) indicated that the secondary amine utilized for metal reduction is the reason for the band's disappearance at 2926cm^{-1}. While the bands that are positioned at 1466.22cm^{-1} belong to the COO^-group. The absorption band detected at 1640.78cm^{-1} corresponds to either the protein amide groups or the carbonyl stretching groups of algal polysaccharides. The band at 1066.15cm^{-1} is attributed to either the CN stretching of the aromatic amine group or the S=O stretch of the sulfated polysaccharides.

The absorption bands located at 835.56cm^{-1} are accounted to (C=O) SO_4 of sulfated polysaccharides'.

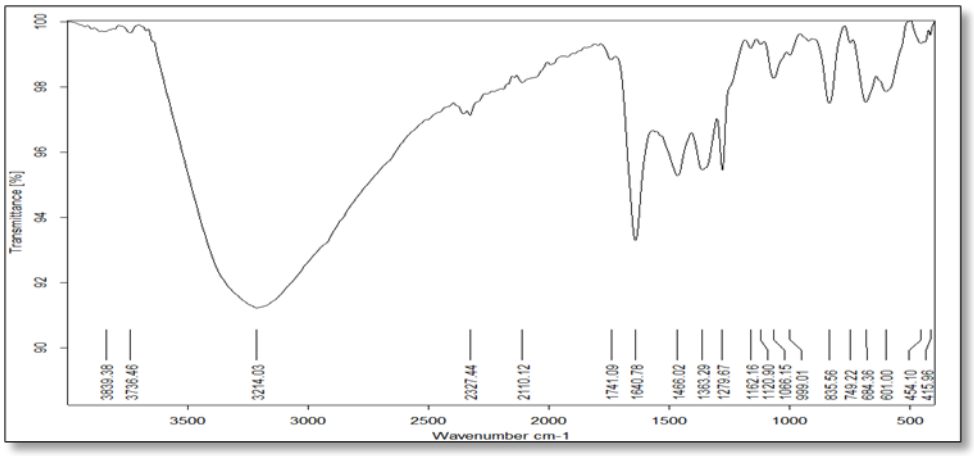

Fig. 5. FT-IR analysis for biosynthesized iron nanoparticles using *Jania rubens* extract

Transmission electron microscope (TEM) of nanoparticles

The TEM image of the different groups of nanoparticles (presented in Figs. 6-9) indicates that the majority of these nanoparticles had spherical shapes and recorded diameters ranging between 2.16 - 4.32nm. The findings of the current study are in agreement with the measurements done by **Ali *et al.* (2011)**. The diameters of the iron nanoparticles that were biosynthesized with various plant extracts ranged from 1.44 – 18.5nm (Fig. 7).

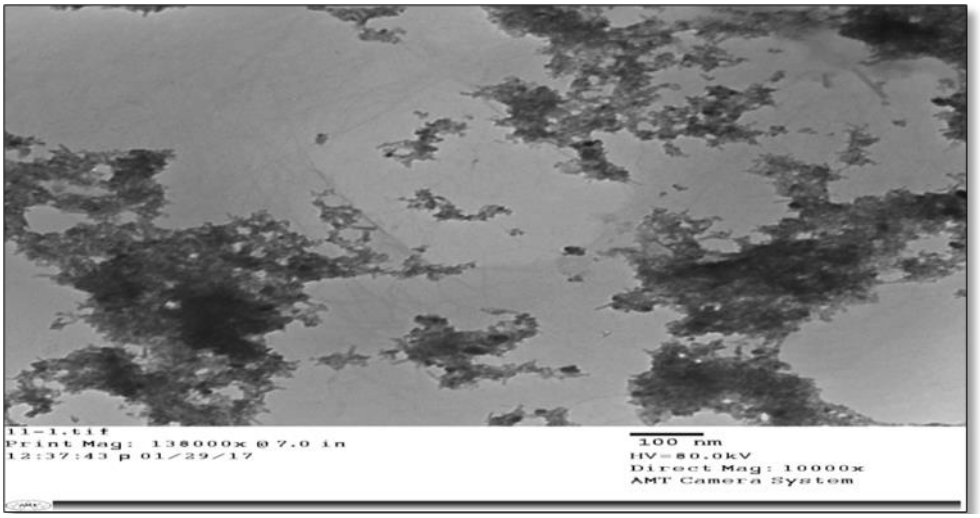

Fig. 6. The TEM micrograph of the synthesized magnetic iron nanoparticles with diameter ranging from 2.6 to 15.2nm

The shape and diameter of each biosynthesized nanoparticle depend on the type of extract, in other words depending on the reducing agent which may be different according to the extracted compounds (see FT-IR results). The extracted compounds from the selected marine algae and mangrove (*Jania rubens, Avicennia marina, Ulva*

fasciata Delile, *Pterocladiella capillacea*, and *Corallina mediterranea*) acts as an efficient stabilizer and reducing agent **(Mahdavi *et al*., 2013)**.

It is easily noticed from Fig. (7) that the formed nanoparticles have an aggregated shape which is consistent with the previously published data **(Peng & Sun, 2007)**. The aggregation is caused by the magnetic attraction forces between the synthesized iron nanoparticles. While the data shown in Fig. (8) presents the TEM images of biosynthesized nano-iron with NaOH as precipitant at pH=9, the measured diameters of biosynthesized iron nanoparticles using plant extract in an alkaline medium ranged from 1.44 to 7.92nm.

As shown in Fig. (8), the aggregated particles were of spherical-like crystals shape, which was consistent with earlier research of **Yang *et al*. (2014)** using NaOH as a precipitant.

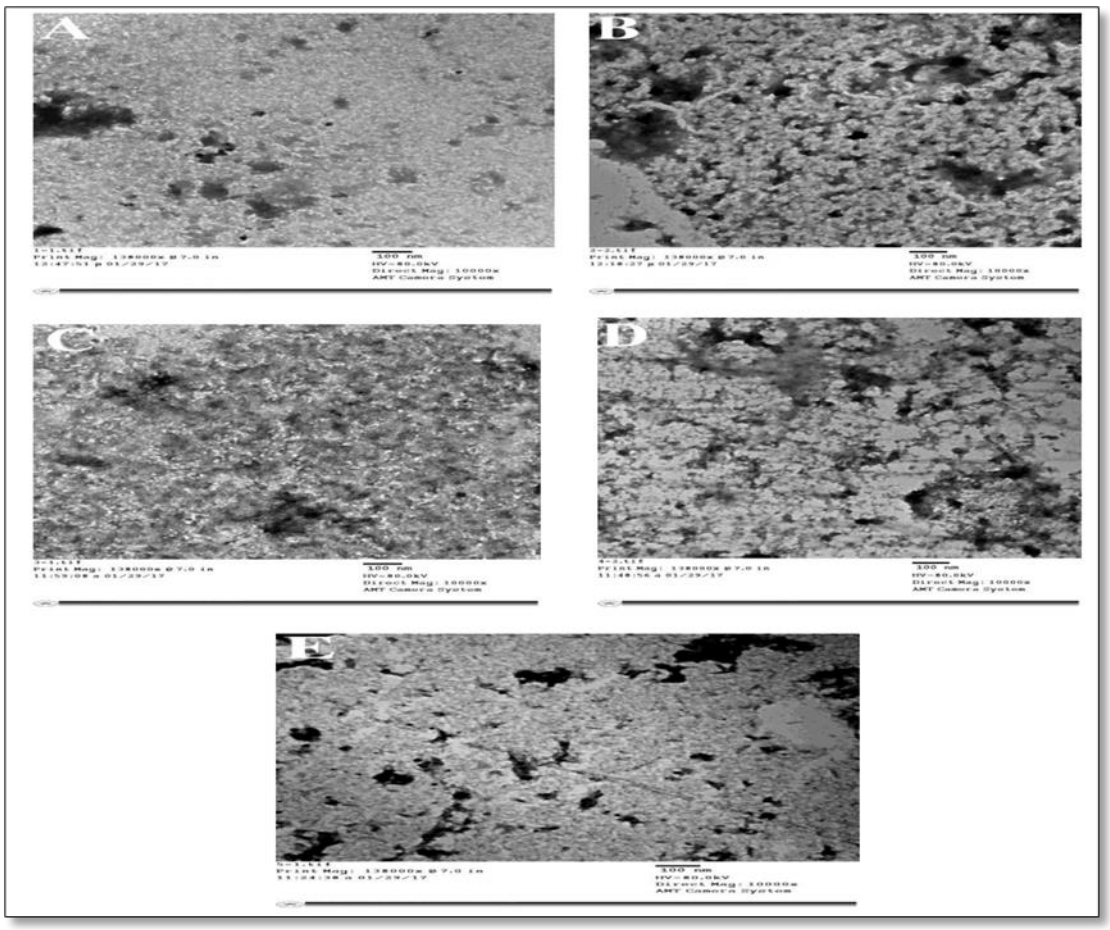

Fig. 7. TEM image of biosynthesized iron nanoparticles using water extract of **A:** *Jania rubens*, **B:** *Avicennia marina*, **C:** *Ulva fasciata* Delile, **D:** *Pterocladiella capillacea*, and **E:** *Corallina mediterranea* Areschoug plants

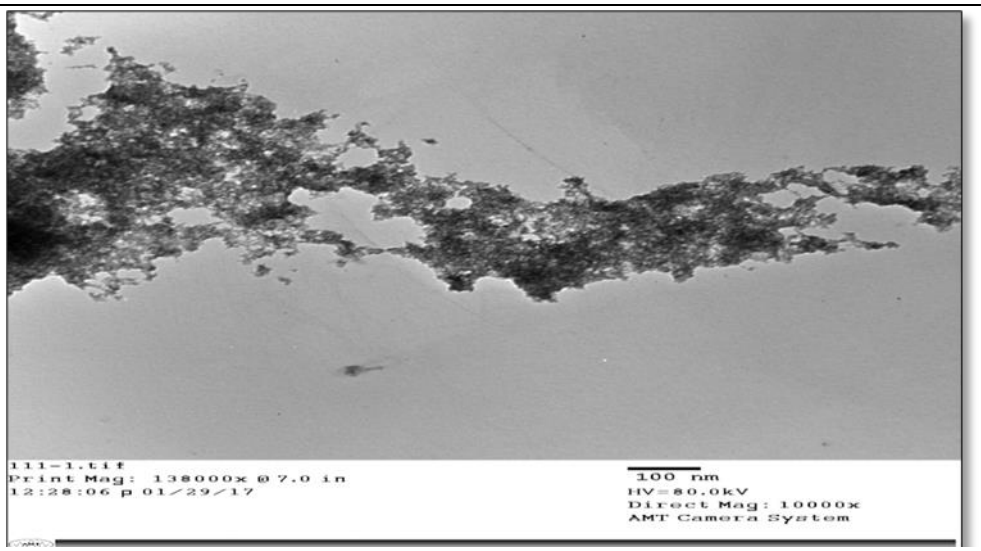

Fig. 8. TEM micrograph of alkaline biosynthesized iron nanoparticles

Fig. (9) displays the chitosan nanoparticles' TEM image. The diameters of the nanoparticles were in a range from 2.16 to 4.32nm. The shape and size recorded in the current study are in high agreement with the previous study by **Ali *et al.* (2011)**, as the majority of these nanoparticles have spherical shapes.

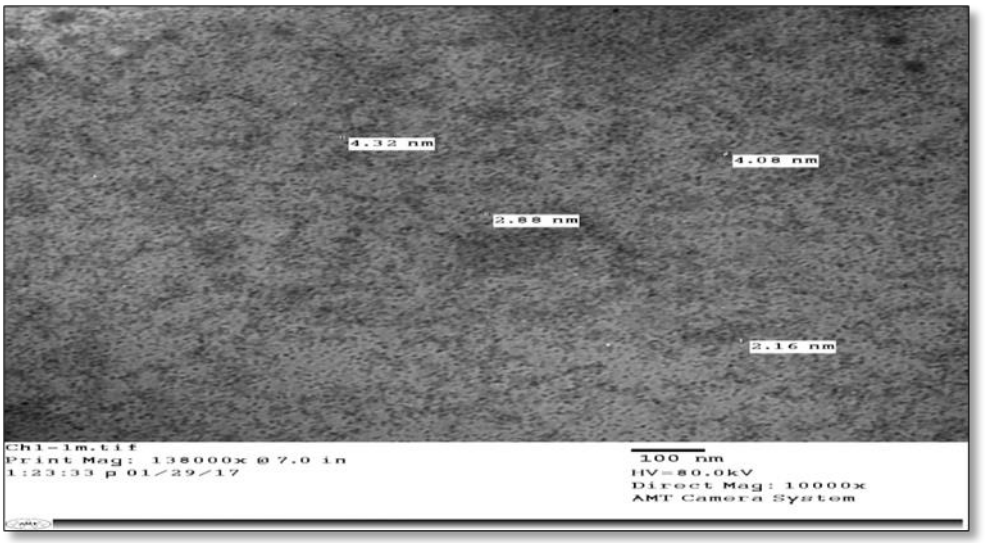

Fig. 9. TEM micrograph of chitosan nanoparticles

Antibacterial activities of crude extracts and biosynthesized nanoparticles

The antimicrobial activity of the crude extracts *(U. fasciata, C. mediterranea, J. rubens, P. capillacea*, and *A. marina)* and consecutive nanoparticles composites of (chitosan, iron, or magnate) with the crude extracts were investigated against the bacterial community collected from Eastern Harbor seawater, Alexandria, Egypt, besides *Escherichia coli* ATCC 19404 and *Staphylococcus aureus* ATCC 6538 as two- reference

strain. The recorded data in Table (1) confirm that the crude algal extract and *A. marina* extracts had low AUs against bacterial community, *E. coli* ATCC 19404 and *S. aureus* ATCC 6538. The crude extracts of both J. *rubens* and C. *mediterranea* exhibited the highest AU (2.8) against *E. coli* ATCC 19404, while *A. Marina* showed the lowest positive records, only against *S. aureus* ATCC 6538 (AU= 1.8). In addition, there were no activities observed in some cases.

Table 1. Antibacterial activity of different crude algal and mangrove extracts

Crude extract	**Antibacterial activity (AU) / reference strains**		
	Sea water community	***E. coli***	***S. aureus***
J. rubens	-	2.8	1.8
U. fasciata Delile	1.8	-	-
P. capillacea	1.8	-	1.8
C. mediterranea	1.8	2.8	-
A. marina	-	-	1.8

Data presented in Table (2) show that the composite of nanochitosan with *J. rubens* extract was the most effective composite in the suppression of the bacterial community of Eastern Harbor (AU = 3.4). Both composites nano-compound of chitosan with the extract of *A. marina* and chitosan mixed with *P. capillacea* extract exhibited low inhibition against *S. aureus* ATCC 6538 (AU = 1.8), but they exhibited the same inhibition against bacterial community of Eastern Harbor. Moreover, there was no activity shown against *E. coli* ATCC 19404, which indicated the low efficiency as an antibacterial of these nano-mixtures.

Table 2. Antibacterial activity of chitosan nanoparticles and chitosan nanoparticles with different algal extracts

Composite	**Antibacterial activity (AU) / reference strains**		
	Sea water community	***E. coli***	***S. aureus***
Chitosan + *J. rubens* extract	3.4	-	-
Chitosan + *U. fasciata* extract	2.8	-	-
Chitosan + *P. capillacea* extract	1.8	-	1.8
Chitosan + *C. mediterranea* extract	1.8	-	-
Chitosan + *A. marina* extract	1.8	-	1.8
Chitosan chemical nano	-	-	-

Data presented in Table |(3) confirm high AUs detected for iron nanoparticles and iron nanoparticles with different algal extracts. Generally, AUs ranged from 1.8 to 4.0. The composite of metal-centered nanoparticles with the extract of either *J. rubens* or *U. fasciata* showed the highest AUs against *E. coli* ATCC 19404 and *S. aureus* ATCC 6538. On the other hand, it was found that the magnet plus any of the five extracts had AUs lower than that were obtained by iron plus any of them. Moreover, the magnet chemical with no reductant did not record any positive result against tested bacteria. On the other

side, the data presented in Table (4) reveal that the AUs at ratios of composites either 1: 2 or 1: 3 were still lower than that obtained with 1:1 iron to extract concentration ratio.

Table 3. Antibacterial activity of iron nanoparticles and magnet nanoparticles with different algal extracts

Composite	Antibacterial activity (AU) / reference strains		
	Sea water community	*E. coli*	*S. aureus*
Iron + *J. rubens* extract	2.3	3.4	4.0
Magnet + *J. rubens* extract	-	-	1.8
Iron + *U. fasciata* extract	2.3	4.0	4.0
Magnet + *U. fasciata* extract	1.8	-	1.8
Iron + *P. capillacea* extract	3.4	2.8	2.8
Magnet + *P. capillacea* extract	1.8	-	-
Iron + *C. mediterranea*	2.8	1.8	1.8
Magnet + *C. mediterranea*	1.8	1.8	-
Iron + *A. marina* extract	3.4	2.3	3.4
Magnet + *A. marina* extract	1.8	1.8	1.8
Magnet chemical with no reductant	-	-	-

Table 4. Antibacterial activity of iron nanoparticles synthesized with different algal extracts concentration ratio

Composite	Algae extract ratio to iron sulphate solution	Antibacterial activity (AU) / reference strains		
		Sea water community(*)	*E. coli*	*S. aureus*
Iron + *J. rubens* extract	1:2	1.8	2.3	-
Iron + *U. fasciata* extract	1:2	2.8	1.8	1.8
Iron + *P. capillacea* extract	1:2	1.8	1.8	-
Iron + *C. mediterranea* extract	1:2	1.8	2.3	-
Iron + *A. marina* extract	1:2	1.8	1.8	2.8
Iron + *J. rubens* extract	1:3	1.8	1.8	-
Iron + *U. fasciata* extract	1:3	1.8	-	-
Iron + *P. capillacea* extract	1:3	1.8	1.8	1.8
Iron + *C. mediterranea* extract	1:3	1.8	-	2.8
Iron + *A. marina* extract	1:3	2.3	-	-
Iron NP (as FCl_3)	-	-	-	-

These results indicate that increasing the concentration of the crude extract by double or triple will negatively affect the antimicrobial efficiency of these nanoparticles, as the centered metal will be surrounded by multi-layer of crude extract. Values shown in Table (5) confirm that the AUs by composites at pH=9 showed low level compared to other records. This could be discussed as increasing alkalinity and pH, which increases the nanoparticles aggregation, and hence decreases efficiency.

Table 5. Antibacterial activity of alkaline iron nanoparticles synthesized with different algal extracts in pH = 9.

Composite	Antibacterial activity (AU) / reference strains		
	Sea water community(*)	***E. coli***	***S. aureus***
Iron + *J. rubens* extract	-	-	-
Iron + *U. fasciata* extract	-	-	-
Iron + *P. capillacea* extract	2.8	-	-
Iron + *C. mediterranea* extract	1.8	-	-
Iron + *A. marina* extract	-	-	-
Iron NP	5.4	5.4	7.1

Considering chitosan nanoparticles, these special and effective biopolymers for a variety of applications have antimicrobial activities and film-forming qualities **(Kumar *et al.*, 2020)**. Particularly, **Tayel *et al.* (2023)** suggested that nano-biotechnological techniques could serve as effective solutions for preventing biofilm formation. Moreover, the antimicrobial activities of chitosan nanoparticles (ChNP) were widely reported for both *in vivo* and *in vitro* studies against bacteria, fungi, yeasts, and microalgae **(Rozman *et al.*, 2023)**. Upon the mechanism of action, unmodified chitosan binds to the outer membrane of Gram-negative bacteria, obstructing its permeability and blocking the membrane permeability, which alters the viability of the cell **(Tachaboonyakiat, 2017)**.

Relating the findings of the current study with the previous studies revealed a good agreement of the effectiveness of synthesized metal-centered nanoparticles from the extract of algae and mangrove as an antifouling substrate. According to the findings of **Abdo *et al.* (2021)**, it was revealed that the biosynthesized ZnO NPs from *Pseudomonas aeruginosa* exhibited an inhibition zone of 12.33 ± 0.9mm, indicating high efficacy against *S. aureus*, whereas in the case of *A. marina*-mediated ZnO NP, the inhibition zone was 9.5 ± 0.5 and 9.0 ± 1mm for two distinct concentrations of *S. aureus*.

Consistently, ZnO nanoparticles (NPs) produced from *A. marina* demonstrated inhibitory zones against three pathogens: *S. aureus* (9.5 ± 0.5mm), *S. mutans* (9 ± 1mm), and *Klebsiella* sp. (7.5 ± 0.2mm). Additionally, Ag/Fe_2O_3 NPs at a concentration of 5 g/mL exhibited a significant antimicrobial effect on *S. aureus*, with a measured inhibition zone of 22.3 ± 0.57mm. Recently, **Tayel *et al.* (2023)** directly phyco-synthesized metal nanoparticles using *Corallina officinalis* extract. The efficacy of all nanocomposites derived from photosynthesized NPs and nano-chitosan against *Salmonella typhimurium*, *Pseudomonas aeruginosa*, *Aeromonas hydrophila*, and *Staphylococcus aureus* was assessed, with each nanocomposite demonstrating superior bactericidal potential, surpassing that of ampicillin.

Furthermore, **Bensy *et al.* (2022)** found that the methanol extract of *Ulva lactuca* exhibited maximum activity against *E. coli* (24 ± 2mm), followed by *Salmonella*

typhimurium (23 ± 1mm), *Bacillus cereus* (19 ± 1mm), *Proteus vulgaris* (17 ± 2mm), and *Staphylococcus aureus* (16 ± 2mm). Remarkably, the antibacterial analysis confirmed that the nanoparticles demonstrated higher activity than the algal extracts. Specifically, the iron nanoparticles showed significant activity against *S. aureus* (24 ± 1mm), *E. coli* (29 ± 1mm), and *S. typhimurium* (31 ± 2mm). These results, along with our findings, clearly demonstrate that biosynthesized nanoparticles from algae extracts with iron or chitosan could serve as highly efficient antibacterial agents against resistant bacteria and biofilm-forming bacteria. Additionally, these synthesized nanoparticles are expected to have significant economic and environmental benefits as eco-friendly and effective antifouling composites.

CONCLUSION

This research investigated the efficacy of chitosan, nano-iron, nanomagnet, and biosynthesized nanocomposites from several algal crude extracts (*U. fasciata, C. mediterranea, J. rubens, P. capillacea*) and leaves of the mangrove *A. marina* against a bacterial community as potential antifouling agents in marine environments. The data indicated that the efficiencies of chitosan, nano-iron, and nanomagnet were quite limited and not comparable to those of the synthesized nanocomposites with algal extracts. Among the nanocomposites with chitosan, *J. rubens* and *C. mediterranea* were found to be the most effective at suppressing the bacterial community, while composites with leaves of *A. marina* and *P. capillacea* exhibited very low efficiency. For metal-centered nanoparticles, the synthesized nanocomposites of iron with *J. rubens* and *U. fasciata* demonstrated the highest antibacterial efficiency, followed by the composite with leaves of *A. marina*. The nanocomposites with magnets showed lower efficiency compared to those with iron. Additionally, the study revealed that increasing the concentration of crude extract did not significantly enhance the efficiency of the nanocomposite. Furthermore, altering the pH to alkaline conditions (pH = 9) resulted in a decrease in the antibacterial efficiency of the biosynthesized nanoparticles.

Statements and Declarations

Funding: This work has received institutional funds from National Institute of Oceanography and Fisheries.

Conflicts of interest/Competing interests: The authors declare that they have no known competing financial interests or personal relationships that could have appeared to influence the work reported in this paper. It has not been published elsewhere and that it has not been submitted simultaneously for publication elsewhere.

Availability of data and material: The data and material are available upon request.

Code availability (not applicable)

Authors' contributions:

Nayrah Shaltout: Lab work, writing the draft

Ehab Beltagy: Lab work, writing the draft

Hassan Abdallah Ibrahim: Lab work, writing the draft
Mohamed A. Aly-Eldeen: Lab work, writing the draft.

REFERENCES

Abdo, A.M.; Fouda, A.; Eid, A.M.; Fahmy, N. M.; Elsayed, A.M.; Khalil, A.M.; Alzahrani, O.M.; Ahmed, A.F. and Soliman, A.M. (2021): Green synthesis of zinc oxide nanoparticles (ZnO-NPS) by Pseudomonas aeruginosa and their activity against pathogenic microbes and common house mosquito, Culex pipiens. Materials (Basel), 14:6983. 10.3390/ma14226983

Abdelsalam, K.M.; Shaltout, N. A.; Ibrahim, H. A.; Tadros, H. R.; Aly-Eldeen, M.A. and Beltagy, E. A. (2022) A comparative study of biosynthesized marine natural-product nanoparticles as antifouling biocides, Oceanologia, 64 (1): 35-49, ISSN 0078-3234, https://doi.org/10.1016/j.oceano.2021.08.004.

Aleem, A.A. (1993). The marine algae of Alexandria, Egypt, 139, Privately published, Alexandria.

Ali, S.W.; Rajendran, S. and Joshi, M. (2011). Synthesis and characterization of chitosan and silver loaded chitosan nanoparticles for bioactive polyester. Carbohydrate Polymers, 83:438–446.

Al-Saif, S.S.; Abdel-Raouf, N.; El-Wazanani, H.A. and Aref, I.A. (2014). Antibacterial substances from marine algae isolated from Jeddah coast of Redsea, Saudi Arabia. *Saudi J.Biol.Sci*. 21:57-64.

Al-Zahrani, F.A.; Salem, S.S.; Al-Ghamdi, H.A.; Nhari, L.M.; Lin, L. and El-Shishtawy, R.M. (2022). Green synthesis and antibacterial activity of Ag/Fe_2O_3 nanocomposite using Buddleja lindleyana extract. Bioengineering (Basel)., 9:452. 10.3390/bioengineering9090452

Bensy, A.V.; Christobel, G.J.; Muthusamy, K.; Alfarhan, A. and Anantharaman, P. (2022). Green synthesis of iron nanoparticles from Ulva lactuca and bactericidal activity against enteropathogens. Journal of King Saud University - Science, 34(3): 101888. https://doi.org/10.1016/j.jksus.2022.101888.

Bhadury, P. and Wright, C.P. (2004). Exploitation of marine algae: biogenic compounds for potential antifouling application. *Planta*, 219: 561–578.

Bouhlal, R.; Haslin, C.; Chermann, J.C.; Colliec-Jouault, S.; Sinquin, C.; Simon, G.; Cerantola, S.; Riadi, H. and Bourgougnon, N. (2011). Antiviral activities of sulfated polysaccharides isolated from *Sphaerococcus coronopifolius* (Rhodophytha, Gigartinales) and *Boergeseniellathuyoides* (Rhodophyta, Ceramiales). *Mar.Drugs.* 9 (7): 1187–1209.

Caroni, A. L.; Lima, C.R.; Pereira, M.R. and Fonseca, J.L. (2009). The kinetics of adsorption of tetracycline on chitosan particles. J. Colloid Interface Sci. 340(2): 182-191.

Confederat, L.G.; Tuchilus, C.G.; Dragan, M.; Sha'at, M. and Dragostin, O.M. (2021). Preparation and Antimicrobial Activity of Chitosan and Its Derivatives: A Concise Review. Molecules, 26: 3694. https://doi.org/10.3390/ molecules26123694

Dayong, S.; Jing, L.; Shuju, G. and Lijun, H. (2008). Antithrombotic effect of bromophenol, thealga-derived thrombininhibitor.*J.Biotechnol*.136:577–588.

Dobretsov, S. and Thomason, J. C. (2011). Biofilms on antifouling coatings: a review. Biofouling, 27(1): 73-88.

El-Naggar, N.E.A.; Shiha, A.M.; Mahrous, H. and Mohammed, A.B.A. (2022). Green synthesis of chitosan nanoparticles, optimization, characterization and antibacterial efcacy against multi drug resistant bioflm-forming *Acinetobacter baumannii*. Scientific Reports, 12:19869

El-Rafie, H.M; El-Rafie, M.H. and Zahran, M.K. (2013). Green synthesis of silver nanoparticles using polysaccharides extracted from marine macro algae / Carbohydrate Polymers, 96: 403–410.

El-Sayed, H. S.; Ibrahim, H. A.; Beltagy, E. A. and Khairy, H. M. (2014) Effects of short term feeding of some marine microalgae on the microbial profile associated with Dicentrarchus labrax post larvae, Egyptian Journal of Aquatic Research, 40 (3):251-260. ISSN 1687-4285, https://doi.org/10.1016/j.ejar.2014.08.001.

Flieger, J.; Pasieczna-Patkowska, S.; Zuk, N.; Panek, R.; Korona-Głowniak, I.; Su´sniak, K.; Pizon, M. and Franus, W. (2024). Characteristics and Antimicrobial Activities of Iron Oxide Nanoparticles Obtained via Mixed-Mode Chemical/Biogenic Synthesis Using Spent Hop (*Humulus lupulus* L.) Extracts. Antibiotics, 13: 111. https://doi.org/10.3390/ antibiotics13020111

Kanchana, A.; Agarwal, I.; Sunkar, S.; Nellore, J. and Namasivayam, K. (2011). Biogenic silver nanoparticles from spinaciaoleracea and lactuca sativa and their potential antimicrobial activity. Digest Journal of Nanomaterials and Biostructures, 6: 1741–1750

Kumar, S.; Mukherjee, A. and Dutta, J. (2020). Chitosan based nanocomposite films and coatings: Emerging antimicrobial food packaging alternatives. Trends in Food Science & Technology, 97: 196-209. https://doi.org/10.1016/j.tifs.2020.01.002.

Mahdavi, M.; Namvar, F.; Bin Ahmad, M. and Mohamad, R. (2013). Green Biosynthesis and Characterization of Magnetic Iron Oxide (Fe_3O_4) Nanoparticles Using Seaweed (Sargassum muticum) Aqueous Extract. Molecules, 18:5954-5964; doi:10.3390/molecules18055954.

Peng, S. and Sun, S. (2007). Synthesis and characterization of monodisperse hollow Fe_3O_4 nanoparticles,"Angewandte Chemie, 46(22):4155–4158.

Predoi, D. (2007). A study on iron oxide nanoparticles coated with dextrin obtained by coprecipitation. Dig J. Nanomater Biostruct, 2: 169–173.

Priyanka, K.R. and Rajaram, R. (2023) A critical review on anticandidal properties of marine plants, Regional Studies in Marine Science, (68):103258, ISSN 2352-4855, https://doi.org/10.1016/j.rsma.2023.103258.

Qi, L.; Xu, Z.; Jiang, X.; Hu, C. and Zou, X. (2004). Preparation and antibacterial activity of chitosan nanoparticles, Carbohydrate Research, 339: 2693–2700.

Rozman, N.A.S.; Yenn, T.W.; Ring, L.C.; Nee, T.W.; Hasanolbasori, M.A. and Abdullah, S.Z. (2019). Potential Antimicrobial Applications of Chitosan Nanoparticles (ChNP). J. Microbiol. Biotechnol. 29(7):1009–1013 https://doi.org/10.4014/jmb.1904.04065

Shaltout, N. A. and Shams El-Din, N. G. (2015). Investigation of the fatty acid profile in some macroalgae in relation to the environmental conditions for biodiesel production. American Journal of Environmental Sciences, 11(6): 402.

Son, S.; Singha, K. and Kim, W.J. (2010). Bioreducible BPEI-SS-PEG-cNGR polymer as a tumor targeted nonviral gene carrier. Biomat. 31: 6344–6354.

Tachaboonyakiat, W. (2017). Antimicrobial applications of chitosan. In Chitosan Based Biomaterials; Jennings, J.A., Bumgardner, J.D., Eds.; Woodhead Publishing: Cambridge, UK, 2: 245–274.

Tang, Z.X.; Qian, J.Q. and Shi, L.E. (2007) Preparation of Chitosan Nanoparticles as Carrier for Immobilized Enzyme. Applied Biochemistry and Biotechnology, 136: 77-96. http://dx.doi.org/10.1007/BF02685940

Tayel, A.A.; Elsayes, N.A.; Zayed, M.M.; Alsieni, M.A.; Alatawi, F.A.; Alalawy, A.I. and Diab, A.M. (2023). Powerful antibacterial nanocomposites from Corallina officinalis-mediated nanometals and chitosan nanoparticles against fish-borne pathogens. Green Processing and Synthesis, 12: 42. https://doi.org/10.1515/gps-2023-0042.

Venkatesan, J.; Qian, Z.J.; Ryu, B.; Kumar, N. A. and Kim, S.-K. (2011). Preparation and characterization of carbon nanotube-grafted-chitosan – Natural hydroxyapatite composite for bone tissue engineering. Carbohydrate Polymers 83: 569–577.

Wang, H.; Lee, S. and Deng, Y. (2019). Ulva lactuca extracts as green and sustainable corrosion inhibitors for mild steel in hydrochloric acid medium. Green Chemistry Letters and Reviews, 12(2): 117-126.

Yang, R.G.; Johnson, M.C. and Ray, B. (1992). Novel method to extract large amounts of bacteriocins from lactic acid bacteria. Applied and environmental microbiology, 58: 3355-3359. doi: 10.1128/AEM.58.10.3355-3359.1992

Yang, X.; Shang, Y.; Li, Y.; Zhai, J.; Foster, N. R.; Li, Y.; Zou, D. and Pu, Y. (2014). Synthesis of Monodisperse Iron Oxide Nanoparticles without Surfactants. 2014(1): Article ID 740856, 5 pages, https://doi.org/10.1155/2014/740856.

Zbakh, H.; Chiheb, H.; Bouziane, H.; Sanchez, V.M. and Riadi, H. (2012). Antibacterial activity of benthic marine algae extracts from the Mediterranean coast of Morocco. J. Microb. Biotech.FoodSci.1:219-228.

Zúñiga-Miranda, J.; Guerra, J.; Mueller, A.; Mayorga-Ramos, A.; Carrera-Pacheco, S.E.; Barba-Ostria, C.; Heredia-Moya, J. and Guamán, L.P. (2023). Iron Oxide Nanoparticles: Green Synthesis and Their Antimicrobial Activity. Nanomaterials, 13:2919. https://doi.org/10.3390/nano13222919